Particle Accelerators
1973, Vol. 4, pp. 195–209

MEASUREMENTS AND CALCULATIONS OF FIELD DISTRIBUTIONS IN SHORT HELICAL RESONATORS†

T. A. TOMBRELLO and K. S. JANCAITIS
California Institute of Technology, Pasadena, California 91109, USA
and
P. J. BENDT, B. H. ERKKILA, and R. H. STOKES
Los Alamos Scientific Laboratory, University of California, Los Alamos, New Mexico 87544, USA

Because of the current interest in short helix resonators for use in heavy ion accelerators, we have made an experimental and theoretical study of several resonator geometries. A new calculational technique has been developed to describe more accurately the boundary conditions imposed by simple shorting planes, which in resonators of $\lambda/2$ electrical length cause major perturbations of the electric field distribution and the resonant frequency. The technique is also capable of simulating other termination conditions, and allows the effect of variable pitch to be included. Comparisons have been made with measured electric and magnetic field distributions and resonant frequencies for a variety of half-wavelength designs. These comparisons demonstrate that the new method of calculation is a significant improvement over the standard sheath model.

1. INTRODUCTION

The use of helical waveguides for accelerating heavy particles has been discussed extensively in the literature.[1-3] Recent interest in this field has been based primarily on the low phase velocities that are possible in these structures, which seem especially appropriate for heavy ion acceleration. Interest in alternating phase focusing, and in building linacs with a variable velocity profile has shown that there are good reasons for constructing the accelerator from separately phased, short structures.[3,4] For helices, the most flexibility is obtained through use of the shortest possible elements, i.e. $\lambda/2$ resonators. A heavy ion accelerator has been proposed by the Los Alamos Scientific Laboratory based on the use of $\lambda/2$ helical resonators operating with independent phasing. Since these short resonators show maximum deviation from the predictions of available models there has been a need for experimental and theoretical studies. In early 1971, a program of helix resonator measurements was started at Los Alamos, with emphasis placed on short resonators which would accelerate heavy ions in the velocity range 2–8 per cent of the velocity of light. Helix resonators with acceptable efficiencies for such slow particles operate at rather low frequencies. The combination of low frequency and small transverse dimensions also makes these resonators attractive possibilities for injectors or post-accelerators for cyclotrons.

† Work performed under the auspices of the U.S. Atomic Energy Commission and supported in part by the National Science Foundation (GP-28027).

The most straightforward mathematical description of the helical waveguide has been obtained using the sheath model, in which the helical coil is approximated by an anisotropic conducting layer of the same pitch as the actual coil.[5,6] Nearly all helix calculations have been based on this model, except for loss calculations where effects due to the finite size of the conductor in the helix are added in the form of local field enhancements.[3,7] It has been shown that the spatial variation of the accelerating field from the sheath model accurately reproduces the measured field shape when the length of the helical coil is large compared to the wavelength of the electromagnetic field in the cavity. The measurements, however, show large deviations near the ends of the coil.[7,8] These deviations must necessarily occur because the coupled TE-TM mode that satisfies the boundary conditions at the helix does not automatically satisfy the boundary conditions at the point where the helix is grounded.

In an attempt to overcome this difficulty, Sierk added decaying waveguide fields (beyond cutoff) to the basic sheath field.[9] Though this technique allows considerable improvement in the value obtained for the lowest resonant frequency, the representation of the electromagnetic field is poor, probably because of convergence difficulties. The individual decaying waveguide field components are not orthogonal to the sheath field, and thus a

unique decomposition of this type is not possible. However, one would expect the nonsheath corrections to be small, and the success of the convergence will be determined mainly by how accurately the added field components provide these corrections.

It is the purpose of this paper to compare a new calculational technique with data from $\lambda/2$ helical resonators, and to demonstrate that a significantly better accuracy can be obtained than with previous calculational methods.

2. EXPERIMENT

A helical resonator is formed by placing a conducting coil inside a concentric conducting cylinder as shown in Fig. 1. For radiofrequency tests, resonators were constructed entirely of copper, and had end plates which were clamped in place during the measurements. To form the helix, a lathe was used to wind copper tubing onto a mandrel. The mandrel had grooves cut with the proper pitch and the conductor was guided onto the mandrel using the axial feed mechanism of the lathe. Resonators A, B, and D used 0.64-cm diameter copper tubing while resonator C used 0.48-cm diameter. Resonators A and B were side-terminated as shown in Fig. 1, using hard solder, and resonators C and D were end-terminated by clamping the helix to the end plates. Many model helix resonators were constructed in order to test their characteristics at low power levels. The data discussed later comes from four of these resonators which were chosen to cover a range of design characteristics.

Measurements of the electric and magnetic fields in the resonators were made at low power levels by a perturbation method.[10] The total E^2 field as a function of position along a path parallel to the z-axis was obtained by pulling a 0.95-cm diameter sapphire bead through the resonator with a nylon thread. Before the bead enters the resonator the oscillator frequency is set exactly equal to the fundamental resonant frequency, so there is no phase difference between the exciting antenna and the resonator electric fields. A vector voltmeter is used to observe the phase shift of the resonator fields relative to the oscillator as a function of bead position. The resonator phase was sampled with a lightly coupled probe inserted through the outer cylindrical wall. The following equation relates the phase shift ζ to E^2 at the location of the bead,

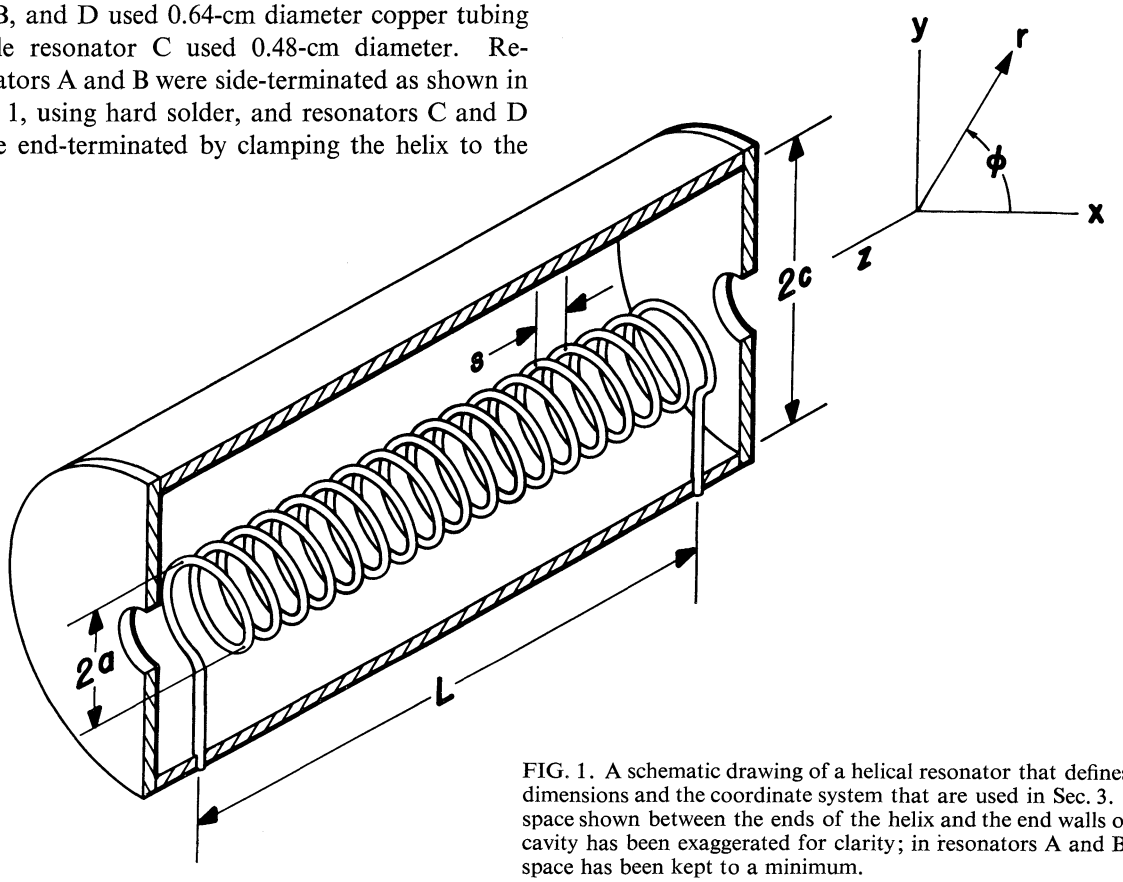

FIG. 1. A schematic drawing of a helical resonator that defines the dimensions and the coordinate system that are used in Sec. 3. The space shown between the ends of the helix and the end walls of the cavity has been exaggerated for clarity; in resonators A and B this space has been kept to a minimum.

$$\tan\zeta = -\frac{3}{2}\omega_0 V\varepsilon_0\left(\frac{\kappa-1}{\kappa+2}\right)\frac{E^2}{P},$$

where ω_0 is the resonant angular frequency, and ε_0 is the dielectric constant of free space. V is the volume of the perturbing bead, κ the specific inductive capacity of the bead, and P is the power dissipated in the resonator. An electric motor drive pulled the bead through the resonator at a constant speed, and a coupled helipot provided a voltage proportional to bead displacement. An X-Y recorder was used to plot the phase shift versus position of the bead. The shunt impedance can be obtained by integrating the square root of $\tan\zeta$ along the resonator axis. Typical values lie in the range 15–25 megohms per meter.

The field components E_z^2, E_r^2, B_z^2, and B_r^2 were determined by pulling 0.84-cm diameter discs of 0.005-cm aluminium foil mounted on nylon threads, along various paths parallel to the axis of the resonator. The discs selectively perturb both the component of the B field perpendicular to the plane of the disc and the components of the E field which are in the plane of the disc. The B field can be distinguished from the E field because the resulting phase shifts have opposite signs. For a given path, phase shifts were measured for three orientations of the aluminium discs perpendicular to the three cylindrical coordinates. Each orientation yielded a curve of phase shift versus z that was a linear combination of the squares of the appropriate field components. Neglecting the effect of E_ϕ^2 and B_ϕ^2, which are expected to be very small, the components E_r^2, E_z^2, B_r^2, and B_z^2 could be obtained by taking differences between the three curves. To obtain accurate results it is essential that the ratio of the thickness to diameter of the perturbing disc be very small (<0.01).[10]

3. THEORY

To describe the helix resonator, we define a cylindrical coordinate system so that the z-axis lies along the common axis of the coil and the outer cylinder; the r and ϕ coordinates then lie in a plane perpendicular to this axis. (Refer to Fig. 1.) The helix has a constant radius a, and the radius of the outer cylinder is c. To support the helical coil, it is either side terminated or end terminated as described in Sec. 2. We mathematically idealize both cases by imposing ground planes at the ends of the helix ($z = 0$ and $z = L$) which cut through the anisotropic conducting layer that represents the coil in the sheath approximation. This mathematical idealization is obviously different from either of the real terminations; the corrections due to such effects will be discussed later in this section.

Because we are chiefly interested in the lowest mode, we consider only those solutions that have no ϕ dependence. (The inclusion of the ϕ-dependent solutions requires only a trivial modification of the following treatment.)

The boundary conditions that **E** and **B** must satisfy in the sheath model[5] are given below.

At $r = c$: $E_z = B_r = E_\phi = 0$.
At $r = a$: $E_z + E_\phi\cot\theta = 0$,
E_z and E_ϕ are continuous,
$B_z + B_\phi\cot\theta$ is continuous,
$(\cot\theta = 2\pi a/s)$.
At $z = 0$ and $z = L$: $E_r = E_\phi = B_z = 0$.

In order to satisfy the boundary conditions exactly at $z = 0$ and L, we choose the following forms for E_z and B_z, with an assumed $e^{i\omega t}$ time dependence:

for $r < a$:

$$E_z(r,z) = \sum_{n=1}^{\infty}\alpha_n I_0(g_n r)\cos\left(\frac{n\pi z}{L}\right),$$

and

$$B_z(r,z) = \sum_{n=1}^{\infty}\beta_n' I_0(g_n r)\sin\left(\frac{n\pi z}{L}\right),$$

for $r > a$:

$$E_z(r,z) = \sum_{n=1}^{\infty}[\gamma_n I_0(g_n r) + \delta_n K_0(g_n r)]\cos\left(\frac{n\pi z}{L}\right),$$

$$B_z(r,z) = \sum_{n=1}^{\infty}[\rho_n I_0(g_n r) + \lambda_n K_0(g_n r)]\sin\left(\frac{n\pi z}{L}\right).$$

The quantity g_n is given by $\sqrt{(n\pi/L)^2-\kappa^2}$ and κ is the free space wave number ($\kappa = \omega/c$). The I_0 and K_0 are the Bessel functions of an imaginary argument. (The standard sheath model treatment[3,6] essentially corresponds to using just the first term in the E_z expression.)

The other components of E and B can easily be obtained from E_z and B_z using Maxwell's equations. For example, for $r < a$:

$$E_\phi(r,z) = -i\kappa \sum_{n=1}^{\infty} \frac{\beta_n'}{g_n^2} I_0'(g_n r) \sin\left(\frac{n\pi z}{L}\right),$$

$$B_\phi(r,z) = i\kappa \sum_{n=1}^{\infty} \frac{\alpha_n}{g_n^2} I_0'(g_n r) \cos\left(\frac{n\pi z}{L}\right),$$

$$B_r(r,z) = -\sum_{n=1}^{\infty} \frac{n\pi}{Lg_n^2} \beta_n' I_0'(g_n r) \cos\left(\frac{n\pi z}{L}\right),$$

and

$$E_r(r,z) = \sum_{n=1}^{\infty} \frac{n\pi}{Lg_n^2} \alpha_n I_0'(g_n r) \sin\left(\frac{n\pi z}{L}\right),$$

where $I_0'(g_n r) = \mathrm{d}I_0/\mathrm{d}r$ evaluated at $g_n r$.

The boundary conditions at $r = c$ relate δ_n to γ_n and λ_n to ρ_n. Then at $r = a$, α_n may be connected to γ_n and β_n' to ρ_n. Finally, the two other conditions at $r = a$ give the following equations:

$$\sum_{n=1}^{\infty} \alpha_n I_0(g_n a) \cos\left(\frac{n\pi z}{L}\right) + (-i\kappa)\cot\theta \sum_{n=1}^{\infty} \frac{\beta_n'}{g_n^2} I_0'(g_n a) \sin\left(\frac{n\pi z}{L}\right) = 0,$$

and

$$\sum_{n=1}^{\infty} \beta_n' \frac{I_0'(g_n c)[I_0'(g_n a)K_0(g_n a) - I_0(g_n a)K_0'(g_n a)]}{[I_0'(g_n a)K_0'(g_n c) - I_0'(g_n c)K_0'(g_n a)]} \sin\left(\frac{n\pi z}{L}\right)$$

$$+ (i\kappa)\cot\theta \sum_{n=1}^{\infty} \frac{\alpha_n}{g_n^2} \frac{I_0(g_n c)[I_0(g_n a)K_0'(g_n a) - I_0'(g_n a)K_0(g_n a)]}{[I_0(g_n a)K_0(g_n c) - I_0(g_n c)K_0(g_n a)]} \cos\left(\frac{n\pi z}{L}\right) = 0.$$

If we multiply the first equation above by $\cos(m\pi z/L)$ and the second by $\sin(m\pi z/L)$ and integrate from $z = 0$ to $z = L$, we then obtain:

$$\alpha_m + \sum_{n=1}^{\infty} Q_{mn}\beta_n = 0,$$

and

$$\beta_m + \sum_{n=1}^{\infty} P_{mn}\alpha_n = 0.$$

In these equations we have replaced $i\beta_n'$ by β_n and

$$Q_{mn} = -\frac{2\kappa}{\pi} \frac{1}{g_n} \frac{I_1(g_n a)}{I_0(g_m a)} G(m,n),$$

$$P_{mn} = \frac{2\kappa}{\pi} \frac{g_m}{g_n^2} \frac{I_0(g_n c)}{I_1(g_m c)} \left[\frac{I_1(g_m c)K_1(g_m a) - I_1(g_m a)K_1(g_m c)}{I_0(g_n a)K_0(g_n c) - I_0(g_n c)K_0(g_n a)}\right] G(n,m)$$

and

$$G(m,n) = \frac{\pi}{L}\int_0^L \cos\left(\frac{m\pi z}{L}\right)\cot\theta \sin\left(\frac{n\pi z}{L}\right)\mathrm{d}z.$$

We now see the advantage of taking separate expansions of E_z and B_z: not only are the boundary conditions at the ends of the helix exactly satisfied, but the boundary conditions at the helix yield a linear set of equations. To find a solution we truncate the summation to N nonzero terms; since the system is homogeneous, the condition that the determinant vanish gives a dispersion relation for the eigenfrequencies. Setting $\alpha_1 = 1$, we can solve for the remaining α's and β's.

It should be noticed that no assumption has been made concerning the z-dependence of $\cot\theta$, so that cases with variable pitch are included automatically. If $\cot\theta$ is symmetric about the center of the cavity, the system splits into two separate homogeneous sets of equations; the even α's couple only to the odd β's and *vice versa*.

The calculation just described considers the expansion of the electromagnetic fields in the full cavity and henceforth will be referred to as the 'full' approximation. As a method of checking the accuracy of this technique, another calculation has been made under more restricted conditions. This second case considers only the fields in half the cavity ($z = 0$ to $z = L/2$), and thus can allow only variations in pitch that are symmetric about the center of the cavity.

This calculation will be referred to as the 'half' approximation. For convenience the point $z = 0$ will now be taken at the center of the cavity; thus, the grounded end is at $z = L/2$. To satisfy the boundary conditions at $z = L/2$, we must now expand E_z in a sine series and B_z in a cosine series. For example, at $r < a$:

$$E_z = \sum_{n=1}^{2N-1} \alpha_n I_0(g_n r) \sin\left(\frac{n\pi z}{L}\right)$$

and

$$B_z = \sum_{n=1}^{2N-1} \beta_n' I_0(g_n r) \cos\left(\frac{n\pi z}{L}\right),$$

where the boundary condition at $z = L/2$ requires that the summations be only over odd n. We now find that a given α_n couples directly to β_n. The α's in the 'full' approximation are simply related to those of the 'half' approximation

$$\alpha_{3,\,\text{full}} = -\alpha_{3,\,\text{half}};$$

$$\alpha_{5,\,\text{full}} = \alpha_{5,\,\text{half}};$$

$$\alpha_{7,\,\text{full}} = -\alpha_{7,\,\text{half}}; \text{ etc.}$$

Up to this point in the development of the theory, no free parameters have been introduced. Thus, having specified the dimensions of the helix the resonant frequencies and the coefficients in the expansions of the fields are uniquely determined.

The corrections due to the way the helix is terminated at the ends of the cavity are easily included in either approximation. Let us consider the following very simplified picture of the departure from the sheath model near the end of the helix in the 'full' approximation:

(1) For *end termination* the current in the coil departs from its spiral pattern and for a short length p runs parallel to the z-axis into the end wall. The correction to $G(m, n)$ from this source may be easily calculated, since over the distance p at each end, $\cot\theta(z)$ is zero. Thus,

$$G(m,n;p) = G(m,n) - \frac{\pi}{L}\left\{\int_0^p \cos\left(\frac{m\pi z}{L}\right)\cot\theta(z)\sin\left(\frac{n\pi z}{L}\right)dz + \int_{L-p}^{L} \cos\left(\frac{m\pi z}{L}\right)\cot\theta(z)\sin\left(\frac{n\pi z}{L}\right)dz\right\}.$$

Assuming $\cot\theta(z)$ is constant over the range of each integration, we obtain for $p \ll L$:

$$G(m,n;p) = G(m,n) - \frac{n\pi^2 p^2}{2L^2}[\cot\theta(0) - (-1)^{n+m}\cot\theta(L)].$$

(2) For side termination the effective change of pitch near the end is much less pronounced than for end termination, but here the current tends toward having only a θ component for a distance p near the termination. We therefore take $\cot\theta(z)$ to be $(p/z)\cot\theta(0)$ and $p(L-z)^{-1}\cot\theta(L)$ within p of the end points at $z = 0$ and $z = L$, respectively. Thus,

$$G(m,n;p) = G(m,n) + \frac{\pi}{L}\left\{\int_0^p \cos\left(\frac{m\pi z}{L}\right)\left(\frac{p}{z}-1\right)\cot\theta(0)\sin\left(\frac{n\pi z}{L}\right)\mathrm{d}z + \int_{L-p}^{L} \cos\left(\frac{m\pi z}{L}\right)\left(\frac{p}{L-z}-1\right)\cot\theta(L)\sin\left(\frac{n\pi z}{L}\right)\mathrm{d}z\right\}.$$

Again assuming $p \ll L$:

$$G(m,n;p) \simeq G(m,n) + \frac{n\pi^2 p^2}{2L^2}[\cot\theta(0) - (-1)^{n+m}\cot\theta(L)].$$

We thus see that the correction term has exactly the same form as in (1) but has the opposite sign. (Similar expressions can be obtained in a straightforward way for the 'half' approximation.) With these pictures in mind we shall investigate the role played by the method of termination by using p as a variable; $p > 0$ referring to case (1) and $p < 0$ referring to case (2).

4. COMPARISON OF THE EXPERIMENTAL AND THEORETICAL RESULTS

In this section we shall compare the calculations described in the previous section with the field measurements discussed in Sec. 2. The dimensions of the resonators and their resonant frequencies in the lowest mode are given in Table I together with the frequency prediction of the standard sheath model. These particular examples were chosen because they show how the electromagnetic properties change with the dimensions and termination. The agreement with our calculations is neither better nor worse for these resonators than for other devices that have not been described in this paper. Thus, these results are typical of a wide range of helical resonator types.

In comparing the calculations to the data we have not taken into account the finite size of the perturbing bead or disk. For most of the results this introduces little error; however, near the end wall of the cavity where the bead or disk begins to enter the exit hole, the measurements are probably appreciably smaller than the actual fields.

In the figures we have chosen to present only the fields in half of each resonator. Since data were available over the whole range in z, the experimental curves shown are averages of the results in the two halves. This was done to eliminate the slight asymmetries (typically a few per cent in the square of the field) that result from imperfections in the winding or positioning of the helix.

4.1. *Resonator A*

Only the axial field, $E_z(0, z)$, and the resonant frequency were measured for this resonator. The experimental value of the axial field is shown in Fig. 2, where it is compared with results given by the two approximations described in the previous section and with that from the standard sheath model. Table II shows how the α's and the calculated resonant frequency depend upon N and p.

The similarity of the results for $N = 5$ and $N = 10$ indicate that the convergence of both approximations is adequate. The dependence of the resonant frequency on p shows that our simplified model for the termination effects actually produces a slight improvement; however, since the value of p deduced in this way is quite small, we shall consider only $p = 0.0$ for the side terminated resonators to avoid introducing a free parameter into the calculations.

It is clear that the 'half' approximation produces slightly better agreement with the data, but that both methods agree quite well and represent a decided improvement over the standard sheath model treatment. The deviation of the calculated curves from the data near the end of the helix (Fig. 2) is a manifestation of the difference between the mathematical and the actual boundary conditions at the termination.

Figures 3 and 4 show the calculated electric and magnetic fields in various parts of the resonator. Overall, the two approximations yield very similar values for the fields; however, one significant region of disagreement must be noted. Because of the difference of the expansions used for B_z in the

TABLE I

Summary of the dimensions for the four helical resonators described in the text. Refer to Fig. 1 for definitions of a, c, L and s and to the text for a description of the types of termination. The quantity L' is the total length of the resonator measured between the inside surfaces of the end plates. Also given are the frequency of the lowest mode, F_{exp}, and the corresponding frequency, F_s, predicted by the *standard* sheath model (Ref. 6)

Cavity	a (cm)	c (cm)	L (cm)	L' (cm)	s (cm)	Termination	F_{exp} (MHz)	F_s (MHz)
A	2.15	7.47	19.82	21.43	0.903	side	86.12	79
B	5.40	16.19	14.60	15.32	1.043	side	49.26	38
C	4.22	12.68	13.92	14.40	0.782	end	53.94	40
D	4.22	12.68	13.92	14.56	1.530	end	103.87	78

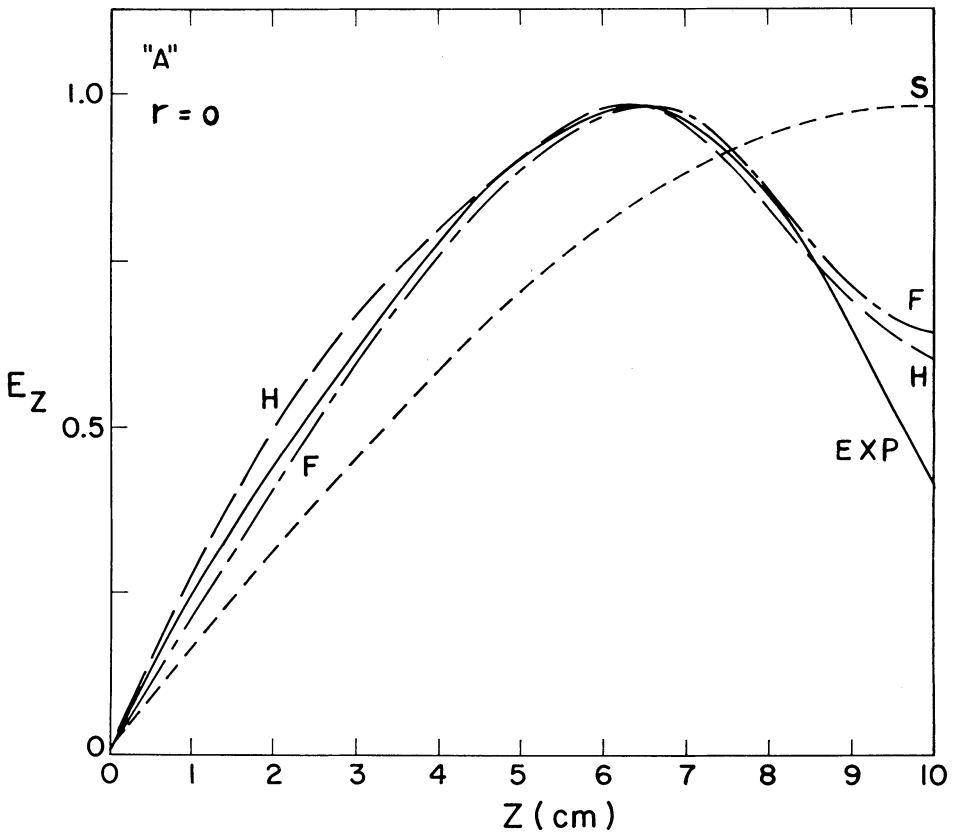

FIG. 2. The z-component of the electric field, $E_z(0, z)$, in cavity A (see Table I for dimensions) along the axis of the cavity. The point $z = 0$ corresponds to the center of the cavity; the helix is grounded at $z = 9.91$ cm. The end wall of the cavity is at $z = 10.8$ cm. The solid curve is the experimental result obtained using a dielectric bead; the dashed curve labeled S is the prediction of the standard sheath model. The curves labeled F and H are the results of using the 'full' and 'half' approximations, respectively. The magnitude of the field is given in arbitrary units and the four curves are normalized so as to give the same value at their maxima. (The F and H curves shown were calculated with $N = 5$ and $p = 0.0$.)

TABLE II

The variation in the calculated resonant frequency, $F_{calc.}$, and the α's with p and N for cavity A using the 'half and 'full' approximations. The measured resonant frequency for this cavity is 86.12 MHz; the predicted frequency from the standard sheath model is 79 MHz. (The curves in Figs. 2, 3 and 4 correspond to $p = 0$ and $N = 5$.)

Approx.	N	p (cm)	$F_{calc.}$ (MHz)	α_3/α_1	α_5/α_1	α_7/α_1	α_9/α_1
'half'	5	−1.0	81.56	0.089	0.004	0.010	0.019
	5	−0.5	86.26	0.214	−0.049	0.041	−0.005
	5	0.0	87.68	0.255	−0.065	0.050	−0.001
	10	0.0	87.20	0.241	−0.055	0.045	−0.008
	5	0.5	89.00	0.294	−0.080	0.058	−0.007
	5	1.0	92.40	0.398	−0.118	0.079	−0.017
'full'	5	−1.0	81.66	−0.043	−0.003	0.004	−0.113
	5	−0.5	86.96	−0.176	−0.068	−0.029	0.001
	5	0.0	88.52	−0.217	−0.088	−0.038	−0.011
	10	0.0	88.16	−0.206	−0.081	−0.034	−0.014
	5	0.5	89.98	−0.258	−0.107	−0.047	−0.011
	5	1.0	93.60	−0.361	−0.151	−0.066	−0.026

two approximations, $B_z(r, z)$ 'half' does not go to zero at the center of the cavity, this causes $B_r(r, z)$ 'half' to be zero on the central plane. This result is clearly an artifact of the 'half' approximation and should be compensated for when loss calculations are made.

Another point that must be considered when the losses are calculated lies in the behavior of B_r near the grounded ends of the helix. Both approximations yield a large peak in B_r in this region; however, in any real resonator (side terminated) in which there is a space between the end of the helix and the cavity wall the field lines will tend to go out the end of the coil before becoming purely radial—thus reducing the size of the peak shown. One must, therefore, view this peak in B_r as also being partially due to the rather artificial boundary condition imposed at the end of the coil.

In Table III the resonant frequency and α's are given for calculations ('full') involving a variable pitch coil in a resonator with the dimensions of A. For this example the pitch variation was assumed to be linear: at $z = 0$, $\cot\theta = (1+\eta)\cot\theta_0$; at $z = L$, $\cot\theta = (1-\eta)\cot\theta_0$; where $\cot\theta_0$ is the actual value of $2\pi a/s$ for resonator A. These results show that the presence of a small antisymmetric component in the pitch (about the center of the cavity) causes the even α's to become nonzero, while the odd α's and the frequency remain close to their original values.

TABLE III

The change in the calculated resonant frequency and α's for cavity A with pitch variation parameter, η. The 'full' approximation was used in both cases with $p = 0$ and $N = 5$

	$\eta = 0.000$	$\eta = 0.10$
$F_{calc.}$ (MHz)	88.52	88.24
α_2/α_1	0.000	−0.081
α_3/α_1	−0.217	−0.213
α_4/α_1	0.000	0.024
α_5/α_1	−0.088	−0.089
α_6/α_1	0.000	0.012
α_7/α_1	−0.038	−0.039
α_8/α_1	0.000	0.006
α_9/α_1	−0.011	−0.018
α_{10}/α_1	0.000	−0.010

4.2. *Resonator B*

The second example shows how the fields change when the radius of the helix becomes larger relative to its length. The experimental and calculated values of the fields are shown in Figs. 5 and 6; the α's and the calculated resonant frequency are given in Table IV.

As described in Sec. 2, the use of a thin, conducting disk for perturbation measurements allows the values of the squares of the individual field amplitudes to be deduced approximately. Since the calculations for this resonator indicate that the ϕ components of the fields should be quite small

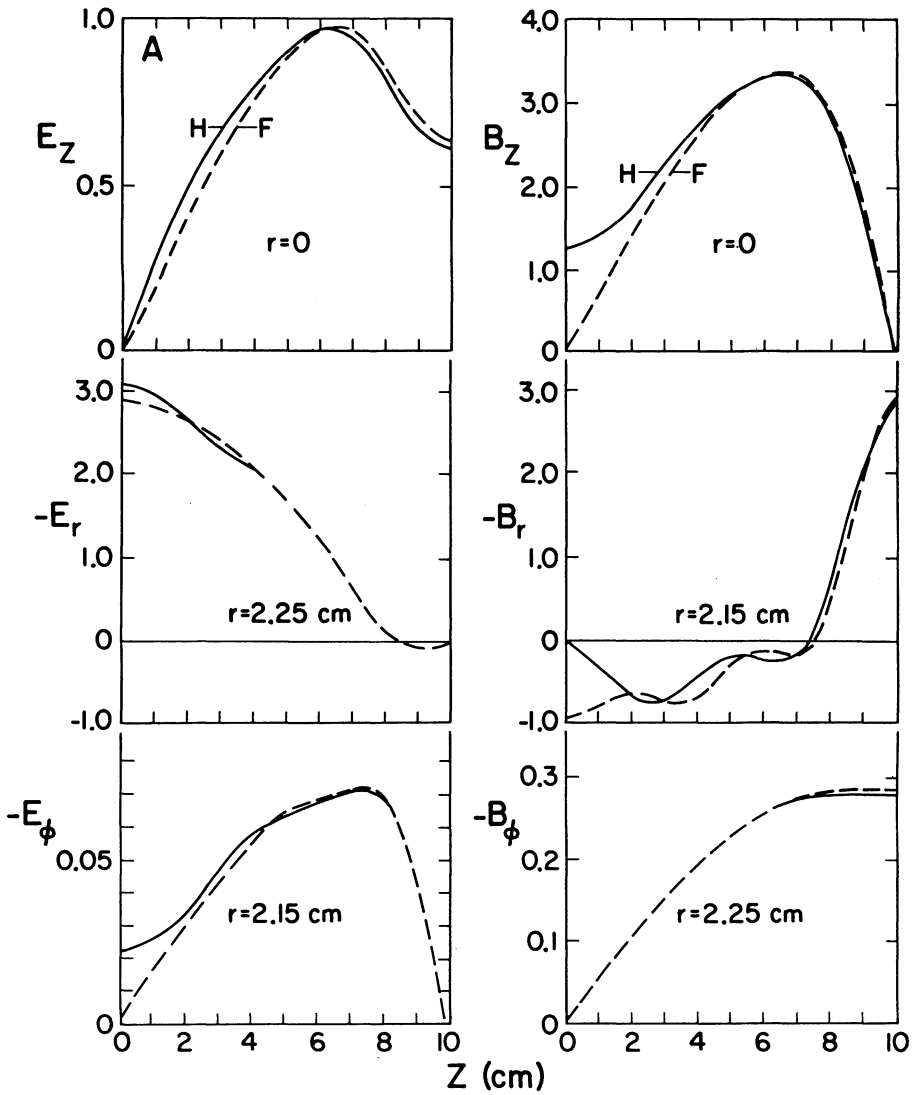

FIG. 3. The calculated behavior of E_z, B_z, E_r, B_r, E_ϕ, and B_ϕ versus z in cavity A. The correct relative magnitudes of the field components are given in arbitrary units. The solid curve corresponds to the 'half' approximation; the dashed curve to the 'full' approximation. Where only one curve is shown the two curves are indistinguishable. (For these curves $N = 5$ and $p = 0.0$.)

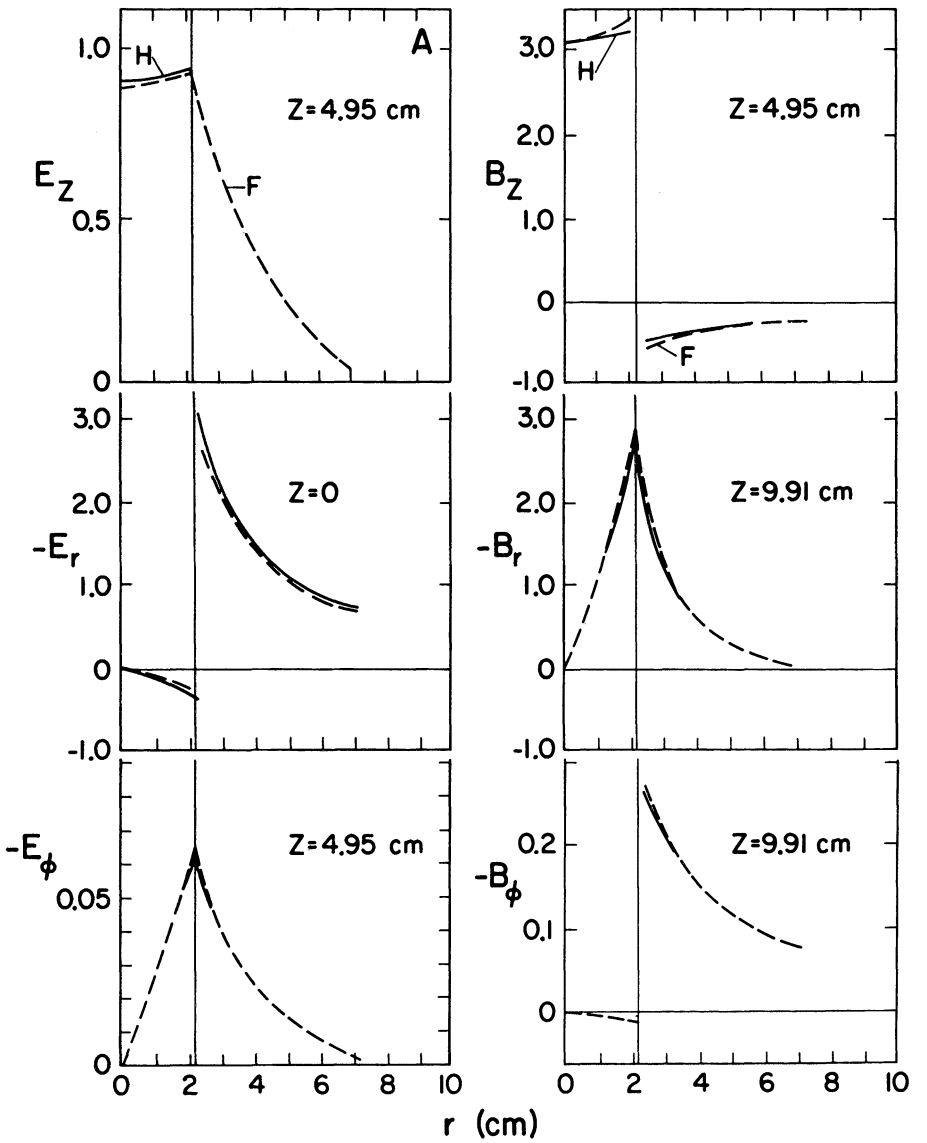

FIG. 4. The calculated behavior of E_z, B_z, E_r, B_r, E_ϕ, and B_ϕ versus r in cavity A. The vertical lines drawn at $r = 2.15$ cm show the radial position of the helix. In all other respects the notation and the relative field strengths follow the same conventions as in Fig. 3.

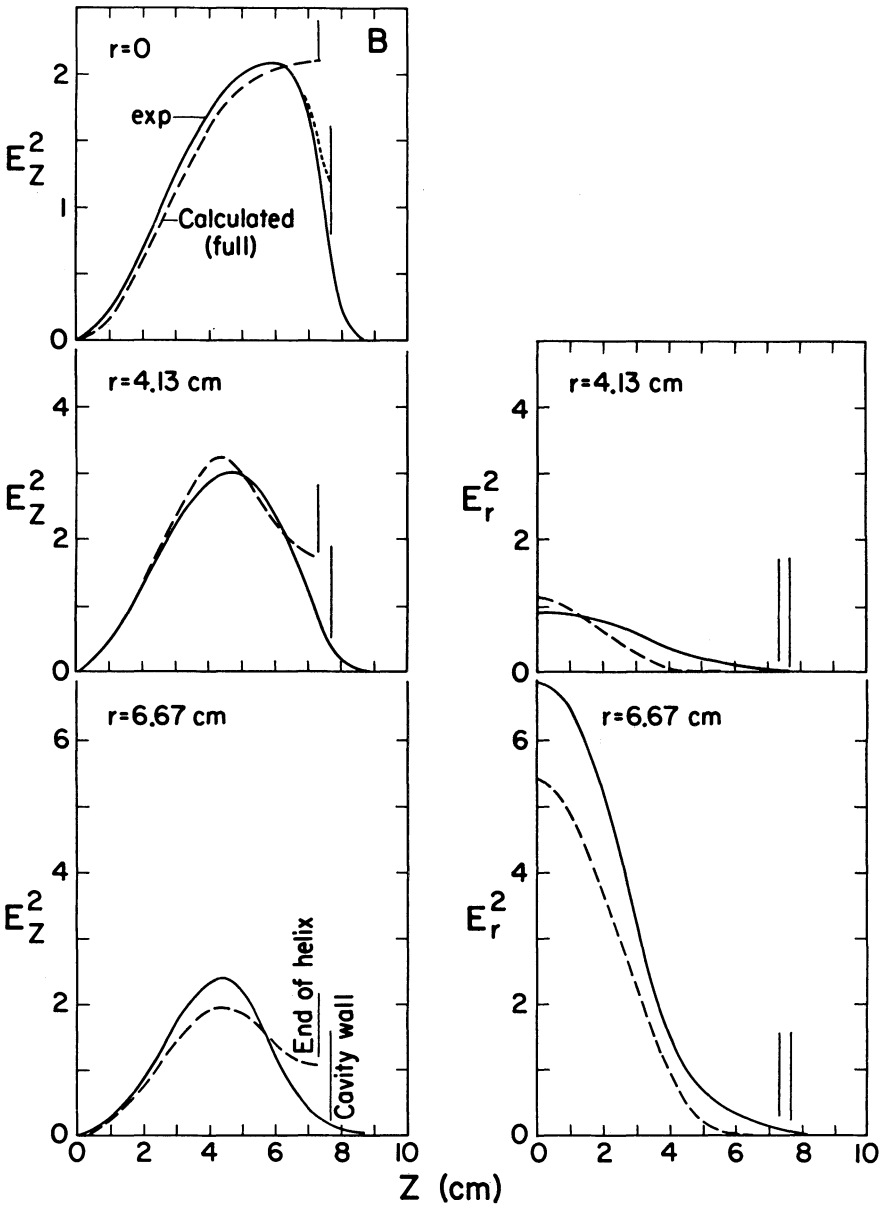

FIG. 5. The experimental values of E_r^2 and E_z^2 for cavity B obtained using the thin disk perturbation method are the solid curves. The dashed curves are the result of the 'full' approximation with $N = 5$ and $p = 0.0$. The normalization of the experimental and theoretical curves was obtained by matching the maxima in $E_z^2(r = 0)$. The vertical lines indicate the positions of the end of the helix and the end wall of the cavity. The vertical scales give the correct relative magnitudes of the fields in arbitrary units. (The dotted addition to the experimental curve for $E_z^2(r = 0)$ represents a crude attempt to correct for the finite size of the disk.)

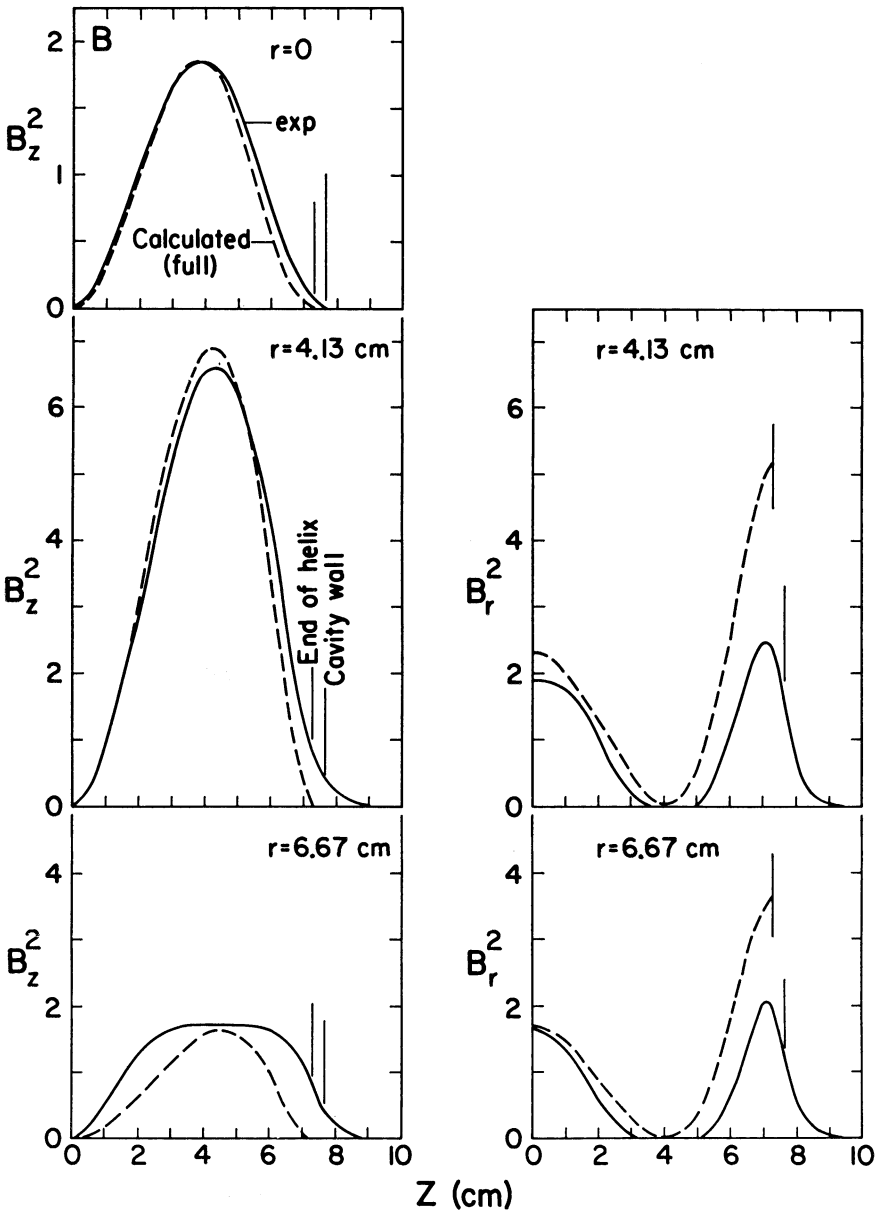

FIG. 6. The experimental values of B_r^2 and B_z^2 for cavity B obtained using the thin disk perturbation method are the solid curves. The calculations shown by the dashed curves use the 'full' approximation with $N = 5$ and $p = 0.0$. The relative normalization of the theoretical and experimental curves was made by matching the maxima of $B_z^2(r = 0)$. The vertical lines indicate the positions of the end of the helix and the end wall of the cavity. The vertical scales give the correct relative magnitudes of the magnetic fields in arbitrary units.

TABLE IV

The resonant frequency and α's for cavities B, C and D for several values of N and p. (Refer to the captions of Tables I and II for the definitions of the F's.)

Cavity	F_{exp}	F_s (MHz)	Approx.	N	p (cm)	F_{calc} (MHz)	α_3/α_1	α_5/α_1	α_7/α_1	α_9/α_1
B	49.26	38	'half'	5	0.0	46.14	0.116	0.001	0.001	0.000
			,,	10	0.0	46.00	0.115	0.001	0.001	0.000
			'full'	5	0.0	51.78	−0.076	−0.004	−0.000	0.000
			,,	10	0.0	51.66	−0.074	−0.004	−0.000	0.000
C	53.94	40	'half'	5	0.0	48.16	0.166	0.001	0.002	−0.000
			,,	5	1.6	52.08	0.252	−0.000	0.003	0.000
			'full'	5	0.0	52.74	−0.112	−0.009	−0.001	−0.000
D	103.87	78	'half'	5	0.0	94.04	0.166	0.001	0.002	−0.000
			,,	5	1.6	101.66	0.251	0.000	0.002	0.000
			'full'	5	0.0	102.98	−0.112	−0.009	−0.001	−0.000

$$(|E_{\phi,\max}(a)|/|E_{z,\max}(0)| \simeq 0.03 \text{ and } |B_{\phi,\max}(a)|/|E_{z,\max}(0)| \simeq 0.07),$$

we have neglected E_ϕ^2 and B_ϕ^2 and used the measurements to determine E_r^2, E_z^2, B_r^2, B_z^2. These results are shown in Figs. 5 and 6 (solid curves), where they are compared with the results of the 'full' approximation. In each figure the calculations are normalized only to the maximum value of the field at $r = 0$; the vertical scales thus give the correct relative magnitudes of the squares of the field components. The 'half' approximation results are not given because 'half' by its nature cannot give a reasonable description of B_r—refer to the discussion on Resonator A. Though $E_z(0, z)$ was slightly better for 'half' than 'full', the curves for E_z^2 and E_r^2 at the two other radii were in significantly better agreement for 'full'.

The fact that the calculated B_r has a larger peak near the end of the helix may result because a few of the magnetic field lines in an actual side terminated resonator are free to emerge from the end of the helix. (Refer to the discussion on Resonator A.) The measured fields shown beyond the end of the helix provide qualitative support of this interpretation. In addition, the magnitudes of the measured fields within 0.4 cm of the end wall of the cavity are strongly affected by the finite size of the disk, because in this region the disk starts to enter the exit hole in the wall. Thus, the actual fields are probably appreciably larger in this region and probably do not drop to zero in the way indicated by the measurements. The shape of the experimental curve for B_z^2 at $r = 6.67$ cm also deviates from the calculated curve. However, since B_z^2 must be extracted from the data after two subtractions, it is not clear that the disagreement is significant.

Though the agreement is far from perfect, with the exception of the peak in B_r near the end of the helix, the theory gives an adequate description of the fields in the resonator. The reader will note that since the squares of the fields are plotted in Figs. 5 and 6, the disagreement between theory and experiment is magnified.

4.3. *Resonators C and D*

Resonators C and D were constructed to determine if terminating the helical coil into the end wall of the cavity would significantly change the properties of a resonator. Though the resonant frequencies given in Table IV agree quite well with those given by the 'full' approximation the axial fields shown in Fig. 7 are poorly described by the calculations. In an attempt to improve the agreement p was varied. (Refer to the discussion at the end of Sec. 3.)

Though one would expect that the optimum value of p would depend on the pitch of the helix, the same value of p was found for both C and D. This value of p (1.6 cm) is somewhat larger than can be justified from the arguments given earlier; thus, one should be wary of associating p with the actual length of a region on the coil. However, it is interesting to note that for the 'half' approximation the resonant frequency peaks at the optimum value

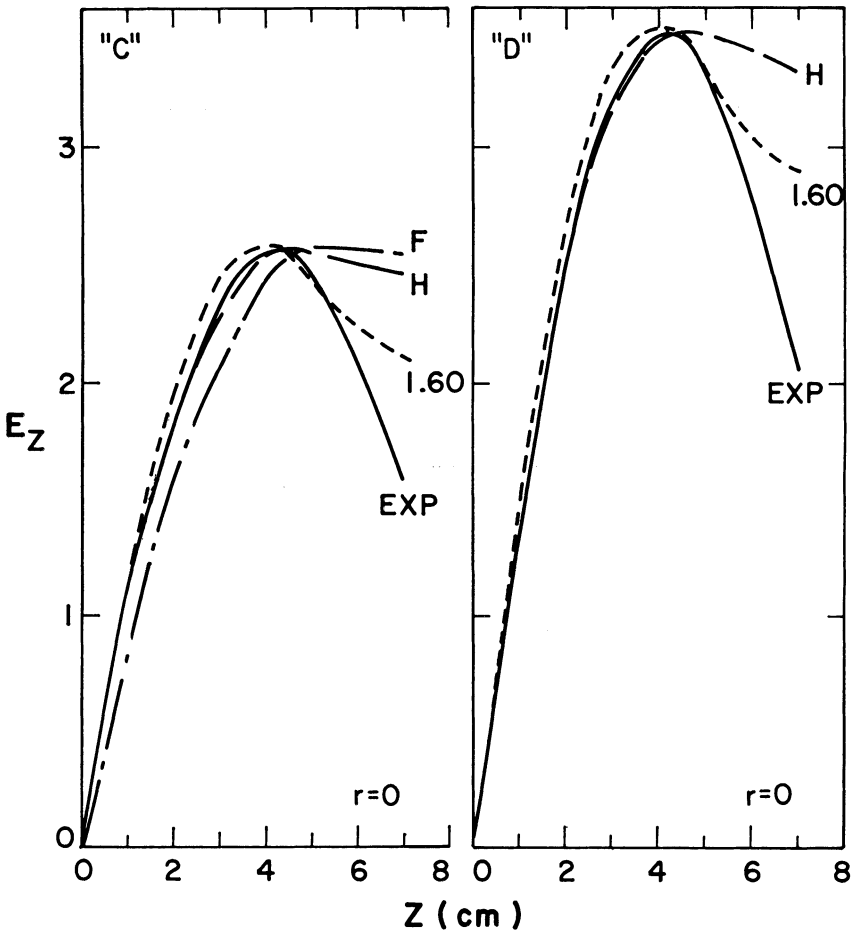

FIG. 7. The z-component of the electric field, $E_z(0, z)$, for cavities C and D along the axis of each cavity. The center of the cavity is at $z = 0$; the end of the helix is at $z = 6.96$ cm. The solid curve gives the experimental value from the dielectric bead method; the curves labeled F and H use the 'full' and 'half' approximations with $N = 5$ and $p = 0.0$. The curve labeled '1.60' gives the result of using the 'half' approximation with $N = 5$ and $p = 1.6$ cm.

of p and that improving the agreement in the frequency also improves the shape of the axial field to a remarkable degree.

5. CONCLUSIONS

The preceding section has shown that the technique described in this paper is a significant improvement over the standard sheath model and allows a reasonably accurate description of the electromagnetic fields in $\lambda/2$ helical resonators. Although it is clear that improvement is still possible, the present results should provide considerable aid in the design of short helical resonators for linacs.

It has been our purpose in this paper to present an extension of the sheath model that allows improved agreement with the experimental data. We have chosen to limit the scope of the presentation to a discussion of the electromagnetic fields, because only by including the field enhancements due to the finite size of the helical conductor[3,7] could we accurately calculate the rf losses and hence determine the Q of the resonator and its shunt impedance. In a future paper we shall consider these loss problems in detail.

ACKNOWLEDGEMENTS

We wish to acknowledge discussions with L. J. Laslett and A. J. Sierk that were very helpful to our understanding of the problem. One of us (T.A.T) wishes to express his appreciation to the Los Alamos Scientific Laboratory for their hospitality during the summers of 1971 and 1972.

REFERENCES

1. W. Muller and J. Rembser, *Nucl. Instr. Meth.*, **4**, 202 (1959).
2. H. Klein, P. Junior, J. Klabunde, O. Siart, H. Deitinghoff, P. Finke, and A. Schempp, *Proc. Int. Conf. on Nuclear Reactions Induced by Heavy Ions* (American Elsevier Publishing Co., New York, 1970), p. 491.
3. A. J. Sierk, C. J. Hamer, and T. A. Tombrello, *Particle Accelerators*, **2**, 149 (1971).
4. I. Ben-Zvi, J. G. Castle, and P. H. Ceperley, *IEEE Trans. Nucl. Sci.*, **NS-19**, No. 2, **226** (1972); H. F. Glavish, *Ibid.*, 307 (1972).
5. J. R. Pierce, *Traveling Wave Tubes* (D. Van Nostrand Co., New York, 1950).
6. J. H. Bryant, *Electrical Communication*, **31**, 50 (1954).
7. H. Klein, N. Merz, and O. Siart, *Particle Accelerators*, **3**, 235 (1972).
8. C. M. Jones, J. P. Judish, R. F. King, S. K. McGowan, W. T. Milner, and P. Z. Peebles, *Particle Accelerators*, **3**, 103 (1972).
9. A. J. Sierk, *IEEE Trans. Nucl. Sci.*, **NS-18**, No. 3, 162 (1971).
10. E. L. Ginzton, *Microwave Measurements* (McGraw-Hill Book Co. Inc., New York, 1957), Chapter 10.

Received 24 October 1972;
in final form 2 January 1973